ACS Pharmacology & Translational Science

pubs.acs.org/ptsci

Open Access

This article is licensed under CC-BY 4.0

Article

Protein Tyrosine Phosphatase 4A3 (PTP4A3) as a Prognostic Biomarker and Pharmacological Target in Acute Myeloid Leukemia

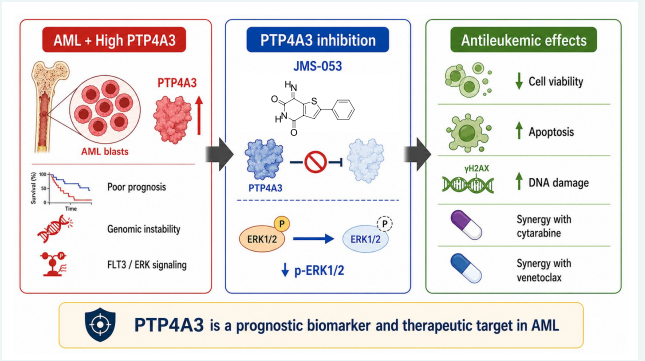
Natália Sudan Parducci,* Maria Fernanda Lopes Carvalho, Isabelle Caroline Santos, Letícia Machado Favery Bertoline, Giovanna A. Castro, Juan Luiz Coelho-Silva, Tiago Agostinho Almeida, Peter Wipf, and João Agostinho Machado-Neto*

Cite This: *ACS Pharmacol. Transl. Sci.* 2026, 9, 3217−3228

Read Online

ACCESS | Metrics & More | Article Recommendations | Supporting Information

ABSTRACT: Acute myeloid leukemia (AML) represents a critical focus for biomarker research, given its high mortality, rapid progression, substantial treatment resistance, and marked genetic heterogeneity. The present study identifies PTP4A3 as a relevant molecular determinant in the disease, linking its overexpression to adverse clinical outcomes, genomic instability, activation of oncogenic signaling pathways, and the expansion of poorly differentiated myeloid populations. The integration of *in silico* analyses with *in vitro* functional assays demonstrated that pharmacological inhibition of PTP4A3 significantly compromises leukemic cell viability and clonogenic potential, while promoting apoptotic signaling and reducing ERK1/2 phosphorylation in a time-dependent manner. The inhibitor JMS-053 showed consistent antileukemic activity across multiple AML cell models and displayed synergistic effects when combined with cytarabine, a cornerstone of current curative regimens. Collectively, these findings support the role of PTP4A3 as both a prognostic biomarker and a promising therapeutic target in AML, providing a rationale for further investigation of PTP4A3-targeted strategies in preclinical and clinical settings.



KEYWORDS: *PTP4A3, Acute Myeloid Leukemia, Prognosis, Treatment Resistance*

Technological advances, particularly the incorporation of artificial intelligence (AI), have endowed oncology research with powerful tools grounded in well-established basic and applied research principles and the expertise of experienced professionals.[1−4] Novel biomarkers for risk susceptibility, diagnosis, prognosis, and stratification have been uncovered as a result of AI's enhanced ability to recognize patterns, correlations, and predictive factors from real-world databases.[5,6] This progress is particularly evident in the context of acute myeloid leukemia (AML),[7,8] a disease arising from the clonal expansion of genetically altered hematopoietic stem and progenitor cells that is responsible for approximately 80% of acute leukemia cases in adults and 15−20% in children.[9]

With the expanding accessibility of *omics* technologies, particularly genomics and transcriptomics, an unprecedented volume of data on tumor biology is being generated; however, the interpretation and integration of these complex data sets pose major challenges for precision oncology.[10] By combining three distinct machine learning (ML) approaches for the analysis of public repositories, Castro et al. (2024)[11] identified genes with significant correlations to AML prognosis. Notably, the gene encoding the phosphatase PTP4A3 (a.k.a. PRL-3) emerges as one of the most strongly associated with survival outcomes. PTP4A3 belongs to the protein tyrosine phosphatase 4A family and is recognized for its dual specificity toward tyrosine and serine/threonine residues.[12,13] Its involvement in tumor progression and malignancy has been demonstrated across multiple neoplasms, including urothelial cancer,[14] colorectal cancer,[15] ovarian cancer,[16] lung cancer,[17] breast cancer,[18] hepatocellular carcinoma,[19] uveal melanoma,[20] renal cancer,[21] and T-cell acute lymphoblastic leukemia.[22] Despite its regulatory roles in apoptosis, epithelial−mesenchymal transition, vascularization,[23] and metastasis[24] in other cancer contexts, as well as its overexpression in approximately half of AML samples and its previously described involvement in FLT3-ITD signaling, cell proliferation, and survival,[25] the

Received: June 21, 2026
Revised: October 8, 2026
Accepted: October 15, 2026
Published: November 2, 2026



ACS Publications

© 2026 The Authors. Published by American Chemical Society

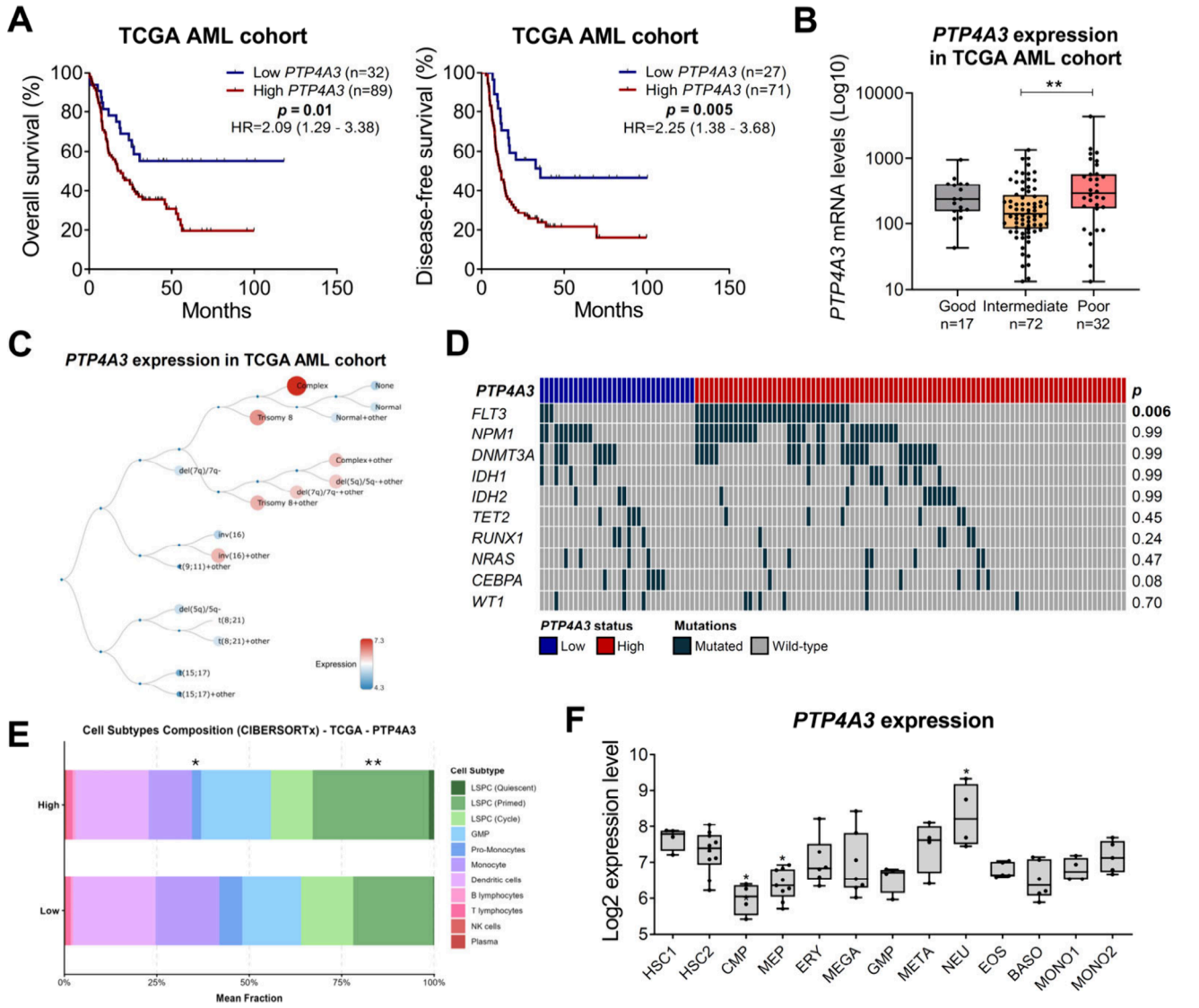


Figure 1. High PTP4A3 expression is associated with poor survival outcomes and adverse clinical features in AML. (A) Survival curves depicting overall and disease-free survival in the TCGA AML cohort stratified by PTP4A3 expression status, demonstrating reduced survival probabilities in patients with higher expression levels. The HR, 95% confidence interval, and *p* values are indicated. (B) PTP4A3 expression levels categorized by AML molecular risk categories. Group comparisons were performed using ANOVA followed by Bonferroni post hoc correction. Survival differences were evaluated by the log-rank test, and hazard ratios were estimated using Cox proportional hazards regression. (C) Hierarchical plots were generated using the BloodSpot platform, with leukemic subtypes exhibiting higher expression of the gene of interest highlighted in red. (D) The dichotomized TCGA cohort was evaluated based on the mutation status of recurrently altered genes in AML, with columns representing patients and rows representing each gene. The presence of a mutation is highlighted in dark gray, and the absence in light gray. (E) The relative fractions of immune/hematopoietic/leukemic cell subtypes inferred using CIBERSORTx based on bulk RNA-seq data. Bars represent the mean proportion of each immune cell population within each group. (F) PTP4A3 expression levels in normal hematopoiesis, calculated based on data made available by the National Center for Biotechnology Information (NCBI, GSE24759). HSC1, hematopoietic stem cell 1; HSC2, hematopoietic stem cell 2; CMP, common myeloid progenitor; MEP, megakaryocyte−erythroid progenitor; ERY, erythrocyte; MEGA, megakaryocyte; GMP, granulocyte−monocyte progenitor; META, metamyelocyte; NEU, neutrophil; EOS, eosinophil; BASO, basophil; MONO1, monoblast; MONO2, monocyte. *$p < 0.05$, **$p < 0.001$.

broader functional consequences of PTP4A3 targeting in AML remain insufficiently characterized.

The investigations presented here were designed to further define the functional relevance of PTP4A3 in AML and to characterize the molecular consequences of its pharmacological inhibition using complementary cell-based and *in silico* approaches. To this end, we employed PRL inhibitors previously synthesized by Rastelli et al. (2021),[26] addressing an important pharmacological gap arising from the lack of clinically available PRL-targeting agents.[27] Given the reported selectivity of these compounds toward PRL phosphatases[28,29] and the emerging involvement of PTP4A3 in key leukemogenic processes,[11] we investigated the therapeutic potential of pharmacological PTP4A3 inhibition in AML. In addition to characterizing the effects of JMS-053 and EJR-925 as single agents, we assessed their combined activity and potential synergistic interactions and performed comprehensive transcriptomic analyses to delineate the molecular programs associated with PTP4A3 inhibition. Collectively, these approaches were designed to expand the understanding of

https://doi.org/10.1021/acsptsci.6c00373
ACS Pharmacol. Transl. Sci. 2026, 9, 3217−3228

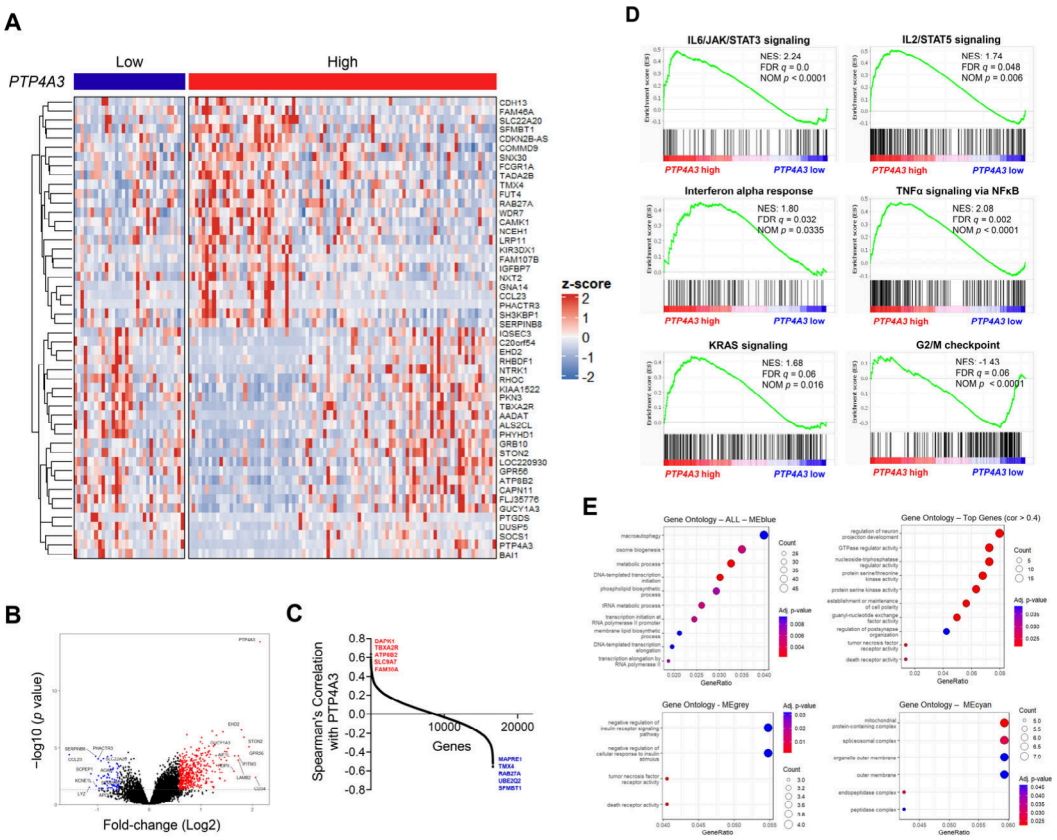


Figure 2. PTP4A3 expression is associated with inflammatory responses, cell cycle progression, transcriptional regulation, and activation of oncogenic signaling pathways. (A) Heatmap constructed using the ClustVis platform, displaying the top DEGs positively and negatively associated with high vs low PTP4A3 expression. (B) Volcano plot and (C) Spearman correlation plot generated using GraphPad Prism 8, illustrating gene sets exhibiting statistically significant log 2-fold change and − log 10 p values. (D) GSEA plots illustrating the continuous Enrichment Scores (ES) for the gene set. (E) GSEAs were conducted using the clusterProfiler R package[2] ($p < 0.05$, FDR < 0.05).

PTP4A3 dependency in AML and to establish the preclinical rationale for its pharmacological targeting.

RESULTS AND DISCUSSION

High PTP4A3 Expression Is Associated with Poor Survival Outcomes and Adverse Clinical Features in AML

The initial screening performed using AI[11] identified PTP4A3 as a gene significantly associated with the prognosis of AML patients. Previously linked to the development of several malignancies, predominantly solid tumors,[14−21] its mapping as a prognostic factor for survival was reinforced by the present study, in which the high expression level of PTP4A3 was associated with poorer overall [hazard ratio (HR) = 2.09, p = 0.01] and disease-free survival (HR = 2.25, p = 0.005) (Figure 1A) and with adverse molecular risk ($p < 0.001$) (Figure 1B) in the AML TCGA cohort treated with curative therapy (cytarabine + anthracycline). The above-described association with patient prognosis was supported by both univariate and multivariate analyses, considering PTP4A3 expression as a categorical and a continuous variable (Tables S1 and S2). Of note, high PTP4A3 as an adverse prognostic marker was further validated in the independent BeatAML cohort (Figure S1A,B).

This prognostic impact extended to cytogenetic classification, with higher PTP4A3 transcript levels associated with trisomy 8 and complex karyotype (Figure 1C), both established markers of poor prognosis.[30] When combined with mutational frequency data, these findings suggest a potential role for PTP4A3 in the maintenance of genomic instability, a process further enhanced by the increased frequency of FLT3 mutations[31] observed in the PTP4A3-high group (Figure 1D). Its association with FLT3 has also been documented in previous studies, which have positioned PTP4A3 as a downstream effector within the FLT3 signaling cascade.[25,32]

In addition to genomic instability, cellular proliferation was identified as a second functional axis influenced by PTP4A3. Beyond its association with increased FLT3 mutations, which promote clonal expansion of leukemic blasts,[33] higher expression levels were detected in quiescent and primed leukemic stem and progenitor cells (LSPCs), as well as in granulocyte−monocyte progenitors (GMPs) (Figure 1E and Table S3). The enrichment of LSPCs in the high PTP4A3 group was also observed in the independent BeatAML cohort (Figure S1C and Table S4). These findings highlight the involvement of PTP4A3 in promoting the proliferation of less differentiated cells, a feature clinically associated with increased chemoresistance.[34] The investigation of PTP4A3 mRNA levels across different stages of myelopoiesis revealed its under-expression in common myeloid progenitors ($p < 0.001$) and megakaryocyte-erythroid progenitors ($p < 0.05$), and its overexpression in neutrophils ($p < 0.05$), relative to hematopoietic stem cells (HSC2) (Figure 1F).

Comparative analysis of gene expression profiles revealed distinct patterns across hematopoietic differentiation stages.

https://doi.org/10.1021/acsptsci.6c00373
ACS Pharmacol. Transl. Sci. 2026, 9, 3217−3228

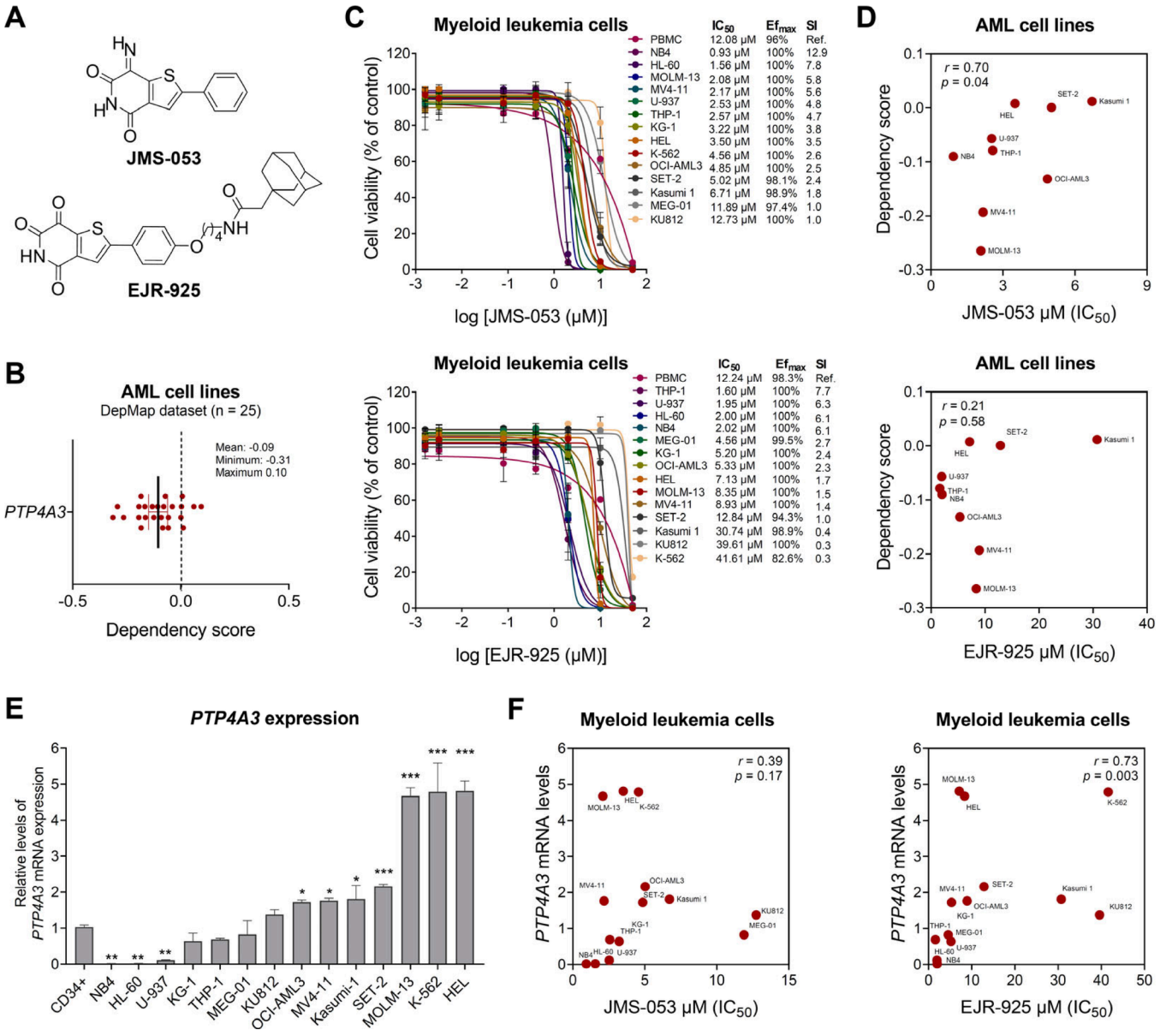


Figure 3. PTP4A3 inhibitors reduce the viability of AML cells. (A) Chemical structure of the PTP4A3 inhibitors JMS-053 and EJR-925. (B) Graph illustrating the PTP4A3 dependency scores, obtained from the DepMap database. (C) Dose-dependent cytotoxicity was evaluated using the MTT assay in a panel of AML cells (MOLM-13, MV4-11, Kasumi 1, OCI-AML3, NB4, KG-1, U-937, THP-1, HL-60, MEG-01, K-562, KU812, SET2, and HEL) and PBMCs. Cell models were exposed to either the vehicle or increasing concentrations of JMS-053 or EJR-925 (0.0032−50 μM) for 72 h. Cell viability was quantified as a percentage relative to that of vehicle-treated controls and used to calculate the SI based on PBMC sensitivity. Results are expressed as the mean ± SD from at least three independent experiments. IC_{50} values are provided in the figure. (D) Scatter plots show the relationship between dependency scores obtained from DepMap CRISPR screening data and IC_{50} values for JMS-053 and EJR-925, derived from MTT cell viability assays, across acute AML cell lines (n = 9; Table S5). Each dot represents an individual cell line, identified by its corresponding name. Spearman' correlation coefficients (r) and corresponding p values are indicated. (E) PTP4A3 gene expression across the AML cell line panel was assessed by quantitative PCR (qPCR), using biological replicates from multiple experiments (n = 3). The p values for each AML cell line vs. $CD34^+$ cells are indicated. *p < 0.05, ** p < 0.01, ***p < 0.001; ANOVA and Bonferroni post hoc test. (F) Scatter plots show the relationship between PTP4A3 mRNA levels obtained from qPCR analysis and IC_{50} values for JMS-053 and EJR-925, derived from MTT cell viability assays, across acute AML cell lines (n = 14). Each dot represents an individual cell line, identified by its corresponding name. Spearman correlation coefficients (r) and corresponding p values are indicated.

Specifically, no statistically significant differences in PTP4A3 expression were observed between hematopoietic stem cells (HSCs) and any of the evaluated AML cytogenetic subgroups, including those characterized by complex karyotypes. Similarly, multipotential progenitors (MPPs) exhibited comparable expression levels across most cohorts, with significant variations restricted to the t(9;11), t(9;22), and t(15;17)/MLL subgroups (Figure S2). In contrast, more committed myeloid progenitors demonstrated pronounced divergence from leukemic cells. Common myeloid progenitors (CMPs) displayed significant differential PTP4A3 expression when compared to the following AML subtypes: t(1;3), abn(3q), del(5q/7q), del(5q), del(7q)/7q−, inv(16), t(9;11), t-(11q23)/MLL, t(15;17), trisomies 8, 11, and 13, and complex

https://doi.org/10.1021/acsptsci.6c00373
ACS Pharmacol. Transl. Sci. 2026, 9, 3217−3228

karyotype. Furthermore, GMPs exhibited the most extensive variance, showing statistically significant differences against normal karyotype (NK), t(1;3), inv(3), abn(3q), del(5q/7q), del(5q), del(7q)/7q−, inv(16), t(6;9), t(8;16), t(8;21), t(9;11), t(15;17), trisomies 7, 8, 11, and 13, as well as complex karyotype (Figure S2). Taken together, these findings indicate that PTP4A3 expression dynamics are strongly associated with the stage of cellular differentiation. The transcriptional profile of PTP4A3 in leukemic blasts diverges more prominently from restricted myeloid progenitors (CMPs and GMPs) than from primitive, immature populations (HSCs and MPPs).

PTP4A3 Expression Is Associated with Inflammatory Processes, Cell Cycle Regulation, Transcriptional Control, And Oncogenic Signaling Pathways in AML

Functional transcriptomic analyses identified a distinct gene expression signature associated with PTP4A3 levels, revealing marked differences between patients with high vs low expression (Figure 2A,C,D). Pathway enrichment analyses supported the involvement of the gene in cellular proliferation, revealing positive associations with increased activation of the IL6/JAK2/STAT3, TNF-α/NF-κB, IL-2/STAT5, and KRAS signaling cascades (Figure 2D), pathways that coordinate apoptotic inhibition and cellular growth and are frequently overexpressed in hematological malignancies.[35−38] The relationship between the activation of inflammatory mediators, including interleukins, and upregulated expression of PTP4A3 is well established in the literature, with several studies validating these findings in B-cell acute lymphoblastic leukemia (B-ALL) models.[39]

Gene Ontology analyses further revealed that genes strongly associated with PTP4A3 expression were predominantly enriched in biological functions related to DNA and RNA processing, GTPase regulatory activity, and tumor necrosis factor receptor activity (Figure 2E). Beyond its previously discussed role in the inflammatory response, the involvement of PTP4A3 in GTPase regulation is supported by studies in AML models demonstrating that PTP4A3 is required to enhance the interaction between mTOR and Rag GTPases, thereby promoting mTOR translocation to the lysosomal membrane.[40] Additional evidence supporting these associations has been reported in other cancer models, including the role of PTP4A3 in RhoA-GTPase activation in hepatocellular carcinoma,[41] regulation of the tumor necrosis factor receptor 1 (TNFR1) feedback loop in breast cancer,[42] and modulation of AKT and mTOR phosphorylation in glioblastoma cell lines.[43] Collectively, these findings provide biological support for the functions identified in our GO analysis. However, they should be considered hypothesis-generating in the context of AML and require further experimental validation.

PTP4A3 Inhibitors Reduce Cellular Viability in a Broad Spectrum of AML Models in a Dose-Dependent Manner

The translation of hypotheses derived from *in silico* analyses into *in vitro* models was conducted using previously described small-molecule inhibitors targeting PTP4A3 (Figure 3A), developed and characterized by Rastelli et al. (2021).[26] Investigations based on the DepMap data set showed that PTP4A3 is not a pan-essential gene in AML cell lines, with dependency scores (DS) predominantly negative or close to zero (Figure 3B). These findings indicate that PTP4A3 dependency is context-dependent, with its depletion promoting cell fitness in some cell lines and having limited effects on viability in others. Thus, the potential therapeutic benefit of targeting PTP4A3 may be restricted to a subset of AML cases. In the cell culture model, the impact of PTP4A3 inhibitors on cell viability was assessed using a methylthiazolyl tetrazolium (MTT) reduction assay (Figure 3C). The variable sensitivity observed across the panel of myeloid neoplasm cell lines is consistent with the context-dependent dependency observed in the DepMap data set. Notably, JMS-053 showed superior efficacy and selectivity compared with EJR-925, supporting its potential as a more effective PTP4A3-targeting compound in susceptible cellular contexts and reinforcing findings previously reported in the literature for solid tumors.[28,44]

Among the most sensitive cell lines were U-937 and HL-60, which were also characterized by the lowest levels of PTP4A3 mRNA expression, and, interestingly, correspond to stages of low hematopoietic differentiation.[45,46] The calculation of the selectivity index (SI), based on the sensitivity of peripheral blood mononuclear cells (PBMCs), revealed distinct selectivity profiles for JMS-053 and EJR-925 across myeloid leukemia cell lines (Figure 3C). JMS-053 exhibited preferential activity against most leukemia cell lines, with the highest SI values observed in NB4 (12.9), HL-60 (7.8), MOLM-13 (5.8), and MV4−11 (5.6), followed by U-937 (4.8), THP-1 (4.7), KG-1 (3.8), and HEL (3.5). Moderate selectivity was observed in K-562 (2.6), OCI-AML3 (2.5), and SET-2 (2.4), whereas Kasumi-1 exhibited a lower SI (1.8). In contrast, MEG-01 and KU812 displayed SI values of approximately 1.0, indicating limited or no preferential selectivity. EJR-925 showed a more heterogeneous selectivity profile, with the highest SI values in THP-1 (7.7), U-937 (6.3), HL-60 (6.1), and NB4 (6.1). Lower but favorable SI values were observed in MEG-01 (2.7), KG-1 (2.4), OCI-AML3 (2.3), HEL (1.7), MOLM-13 (1.5), and MV4−11 (1.4). Conversely, SET-2 exhibited an SI of approximately 1.0, while Kasumi-1 (0.4), KU812 (0.3), and K-562 (0.3) displayed SI values below 1.0, indicating a lack of preferential sensitivity relative to PBMCs. Collectively, these findings demonstrate compound- and cell line-dependent differences in selectivity, with JMS-053 exhibiting a broader preferential activity profile than EJR-925. However, these results should be interpreted as preliminary evidence of selectivity, as the PBMC analysis was performed using cells from a single healthy donor.

Combined with the viability data, further experiments revealed that the sensitivity of AML cell lines to the PRL inhibitor JMS-053, but not to EJR-925, correlates with PTP4A3 dependency scores, indicating a functional association between PTP4A3 dependency and JMS-053 response (r = 0.70; p = 0.04; Figure 3D and Table S4). PTP4A3 mRNA expression profiling across myeloid leukemia cell lines revealed marked variability in transcript abundance, with OCI-AML3, MV4−11, Kasumi-1, SET-2, MOLM-13, K-562, and HEL cells exhibiting significantly higher expression than normal $CD34^+$ cells (all $p < 0.05$; Figure 3E). Across the cell-line panel, PTP4A3 mRNA expression positively correlated with EJR-925 IC_{50} values (r = 0.73; p = 0.003; Figure 3F), indicating that higher PTP4A3 expression was associated with the need for higher concentrations of EJR-925 to reduce cell viability by 50%, consistent with lower sensitivity to the compound.

After identifying THP-1, U-937, and HL-60 as the cell lines most sensitive to the pharmacological effects of both inhibitors, additional viability assays were performed. The efficacy of both treatments did not vary in a time-dependent manner, as shown in Figure S3. The IC_{50} values obtained at 24 h were similar to

https://doi.org/10.1021/acsptsci.6c00373
ACS Pharmacol. Transl. Sci. 2026, 9, 3217−3228

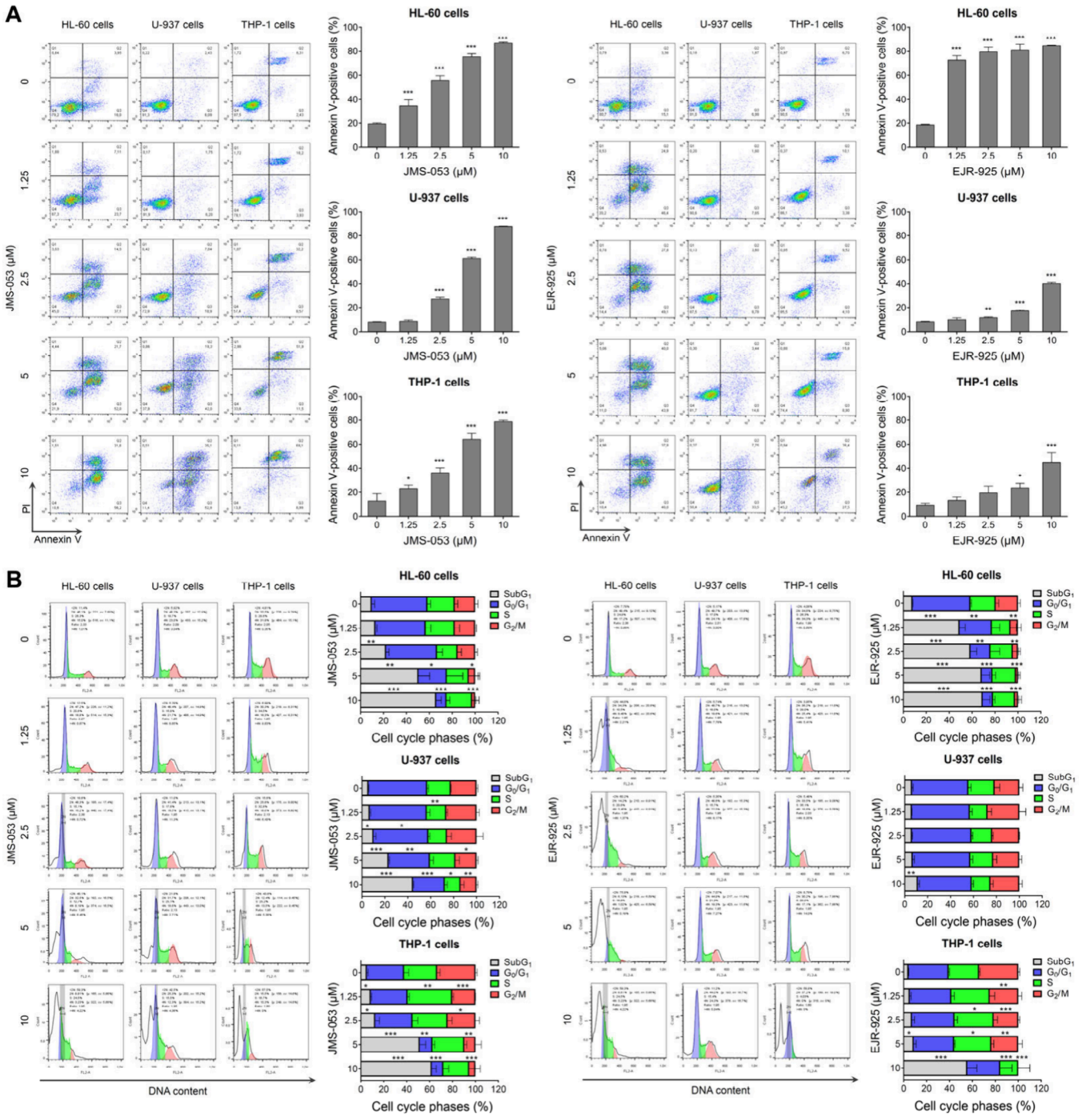


Figure 4. PTP4A3 inhibitors increase apoptotic rate and $SubG_1$ cell population in HL-60, U-937, and THP-1 cells. (A) AML models were treated with the vehicle or JMS-053/EJR-925 for 48 h. Representative dot plots were constructed for each condition, illustrating annexin V-positive cells in the upper and lower right quadrants. Bar graphs represent the mean ± SD of at least three independent experiments. (B) AML models were treated with the vehicle or JMS-053/EJR-925 for 48 h and stained with propidium iodide. Bar graphs represent the mean ± SD of at least three independent experiments, indicating the percentage of the cell population in $SubG_1$, G_0/G_1, S, and G_2/M phases. p values for control vs treated groups for each condition are indicated. *$p < 0.05$, **$p < 0.01$, ***$p < 0.001$; ANOVA and Bonferroni post hoc test.

those observed at 72 h, displaying viability curves with inflection points at the same doses across all treated groups.

Pharmacological PTP4A3 Inhibition Impacts Apoptosis, Cell Cycle-Related Responses, and Clonogenicity in AML Cell Lines

The combination of annexin V and propidium iodide staining demonstrated the efficacy of the compounds JMS-053 and EJR-925 in inducing apoptotic cell death, particularly in HL-60 cells. This cell line exhibited a significant increase in annexin V-positive cells at the 1.25 μM dose ($p < 0.001$), showing greater sensitivity to the EJR-925 inhibitor. The remaining cell lines (THP-1 and U-937) became more responsive at 2.5 μM for JMS-053 ($p < 0.001$) and at 5 μM for EJR-925 ($p < 0.05$) (Figure 4A).

The cell cycle assay further corroborated the previous findings, showing an accumulation of cells in the $SubG_1$ phase

https://doi.org/10.1021/acsptsci.6c00373
ACS Pharmacol. Transl. Sci. 2026, 9, 3217−3228

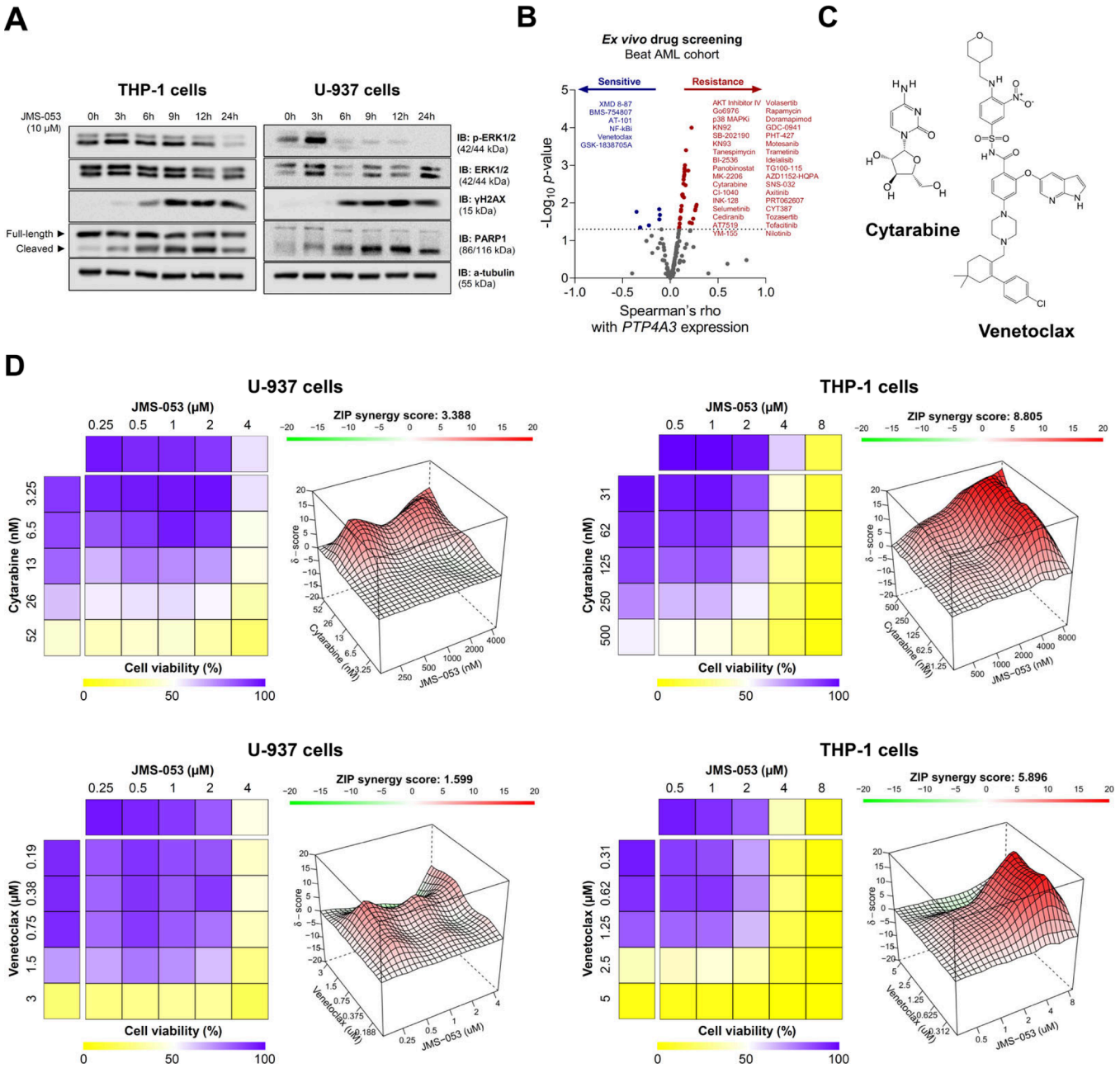


Figure 5. PTP4A3 inhibition attenuates ERK1/2 signaling and enhances the antileukemic activity of cytarabine and venetoclax. (A) Western blot analysis was performed to detect phospho (p)-ERK1/2, ERK1/2, γH2AX, PARP1, and α-tubulin in total cell extracts from THP-1 and U-937 cells treated with JMS-053 (10 μM) for 0, 3, 6, 9, 12, and 24 h. The proteins and the cell lines analyzed are described in the figure. (B) Volcano plot representing the association between PTP4A3 mRNA levels and drug responses. *Ex vivo* drug screening data were extracted from the Beat AML cohort. The *x* axis represents Spearman's *r* values, and the *y* axis represents $-\log_{10}(p \text{ value})$. Negative correlations indicate increased drug sensitivity associated with higher PTP4A3 expression, whereas positive correlations indicate drug resistance ($p < 0.05$). (C) Chemical structure of cytarabine and venetoclax. (D) Dose−response cytotoxicity assays for JMS-053 (0−8 μM for THP-1; 0−4 μM for U-937) combined with venetoclax (0−5 μM for THP-1; 0−3 μM for U-937) or cytarabine (0−500 nM for THP-1; 0−52 nM for U-937) were conducted using the MTT assay in THP-1 and U-937 cells. AML cells were exposed to the vehicle or graded concentrations of the compounds, either alone or in combination, for 72 h. Values are expressed as the percentage of vehicle-treated cells. The ZIP synergy score was calculated using SynergyFinder software (https://synergyfinder.fimm.fi/). Results represent the mean of at least three independent experiments.

following treatment, with a more pronounced effect observed for JMS-053. HL-60 cells exhibited greater sensitivity to EJR-925 treatment (Figure 4B). Beyond the increase in the $SubG_1$ population, treatment with the PTP4A3 inhibitors also altered the distribution of cells across the different cell-cycle phases. A progressive reduction in the proportion of cells in the G_2/M phase was observed with increasing inhibitor concentrations, suggesting that PTP4A3 inhibition may affect cell-cycle progression in addition to inducing apoptosis. These findings are consistent with previous studies implicating PTP4A3 in cell-cycle regulation through the p53 and PI3K/AKT pathways.[17,47] Similarly, PTP4A3 knockdown in breast cancer cell lines resulted in rapid G_1 cell-cycle arrest and induction of a strong TNFα cytokine response,[42] accompanied by a

https://doi.org/10.1021/acsptsci.6c00373
ACS Pharmacol. Transl. Sci. 2026, 9, 3217−3228

significant reduction in the proportion of cells in the S and G_2/M phases.[18]

Colony formation was attenuated at concentrations above 10 μM for JMS-053 and above 20 μM for EJR-925, confirming the superior potency of JMS-053 in THP-1 and U-937 cells (Figure S4). Collectively, these findings support a role for PTP4A3 in promoting cell proliferation and suppressing apoptosis, consistent with evidence reported in previous studies.[32,48]

PTP4A3 Inhibition Reduces ERK1/2 Activation and Potentiates the Antileukemic Effects of Cytarabine and Venetoclax

Given the already high sensitivity of the HL-60 cell line to both compounds under investigation, Western blot and synergy assays were conducted exclusively in U-937 and THP-1 cells. The investigation of the protein panel after JMS-053 treatment revealed a regulatory effect of these compounds on the ERK1/2 pathway. The molecule reduced the levels of phosphorylated ERK1/2 (active form) after 12 h, while promoting a time-dependent increase in cleaved PARP1 and γH2AX, markers of cell death and DNA damage, respectively (Figure 5A). Its involvement in the MAPK cascade via ERK1/2 has also been reported in MOLM-14 cells, in which PTP4A3 overexpression correlated with increased ERK1/2 phosphorylation and, consequently, with treatment resistance, enhanced cell proliferation, and inhibition of apoptosis.[25]

Next, we investigated whether PTP4A3 mRNA expression is associated with the response to antineoplastic agents in AML models. In drug sensitivity assays using primary AML samples from the BeatAML study, PTP4A3 mRNA levels were positively correlated with resistance to 34 compounds and negatively correlated with resistance to six compounds (all $p < 0.05$, Figure 5B). Collectively, these findings suggest that elevated PTP4A3 expression is predominantly associated with chemoresistance in AML. Subsequently, we investigated the impact of combining JMS-053 with clinically relevant agents used in AML therapy, namely, cytarabine and venetoclax (Figure 5C). In THP-1 and U-937 cells, JMS-053 enhanced the antileukemic effects of both cytarabine (ZIP score: 3.38−8.80) and venetoclax (ZIP score: 1.59−5.89), with the strongest effects observed in THP-1 cells (Figure 5D).

The difference in susceptibility to combination therapy between the two cell lines may reflect differences in their dependence on PTP4A3-regulated Mg^{2+} homeostasis. Given the reported interaction between PTP4A3 and CNNM family magnesium transporters, it is possible that PTP4A3 inhibition may influence Mg^{2+} homeostasis and, consequently, mitochondrial function, potentially affecting the cellular response to cytarabine and venetoclax.[49,50] However, as intracellular Mg^{2+} levels, mitochondrial function, and CNNM expression were not assessed in the present study, this mechanism remains speculative. Further studies investigating these variables will be required to determine whether the mechanisms contribute to the differential synergistic responses observed between THP-1 and U-937 cells.

MATERIAL AND METHODS

Transcriptomic Profiling from Public Databases

Genetic and clinical data from non-M3 AML patients who received curative-intent therapy in the Cancer Genome Atlas AML study (n = 121) and BeatAML (n = 199) were retrieved from cBioPortal (https://www.cbioportal.org/). Gene expression data were analyzed as either continuous or categorical variables. Dichotomization was performed based on receiver operating characteristic (ROC) curve analysis, considering the area under the curve (AUC) and the concordance index (C-index), using an optimal cutpoint determined by a maximization metric implemented in the R package Cutpointr.[51] PTP4A3 gene expression was evaluated across different myeloid cell populations using the GSE24759 data set obtained from the GEO2R platform (https://www.ncbi.nlm.nih.gov/geo/geo2r). Within the leukemic cohort, hierarchical plots were generated using the BloodSpot platform (https://www.fobinf.com/) to associate PTP4A3 expression with multiple genetically based classifications of the disease. A comparative transcriptomic analysis was performed to evaluate the expression of PTP4A3 between normal hematopoietic and AML cohorts. Data were obtained from public data sets via the FOBInf platform, including normal samples from GSE42519 and AML samples from GSE13159, GSE15434, GSE61804, GSE14468, and The Cancer Genome Atlas (TCGA) repository.

Gene Set Enrichment Analysis (GSEA)

Clinical and gene expression data were collected from the cBioPortal platform, selecting the acute myeloid leukemia from the TCGA cohort treated with curative-intent therapy (n = 121) as the reference. Molecular interaction investigations were performed using Gene Set Enrichment Analysis (GSEA v.4.0; Broad Institute), measuring correlations based on normalized enrichment score (NES), false discovery rate (FDR), and p values, defined from gene sets curated by MSigDB Hallmarks, Reactome, and KEGG. Enrichment scores (ES) were calculated using the Kolmogorov−Smirnov statistics, tested for significance by 1000 permutations, and normalized to adjust for gene set size. An FDR q-value cutoff below 0.25 was set for significance.

Functional Genomics

Quantile-normalized gene expression was used to generate classifications linked to the limma-voom package in Galaxy Analysis (https://usegalaxy.org/), based on comparisons between high and low PTP4A3 expression groups. Differentially expressed genes (GEGs; FC > 1; $p < 0.05$) obtained from Galaxy were used for Spearman's correlation analysis and for the construction of a volcano plot. A heatmap was generated using ClustVis (https://biit.cs.ut.ee/clustvis/) to illustrate the 50 most DEGs between high and low PTP4A3 expression samples.

Cell-type composition was estimated using the CIBERSORTx platform (https://cibersortx.stanford.edu/) based on transcriptomic data from the TCGA AML (n = 121) and the BeatAML (n = 199) cohort. The inclusion criteria were patients with de novo non-APL AML who received curative-intent therapy with a 7 + 3 regimen and had available gene expression data. Differential gene expression analysis between PTP4A3 groups (high vs. low) was performed using RPKM-normalized gene expression data from the TCGA cohort. Gene coexpression networks were constructed using the Weighted Gene Coexpression Network Analysis (WGCNA) R package.[52] The TCGA mRNA expression cohort was used to identify coexpression modules and candidate genes highly correlated with PTP4A3. To investigate the biological significance of these modules and top correlated genes, Gene Ontology (GO) enrichment analyses were conducted using the clusterProfiler R package,[53] with significance thresholds set at $p < 0.05$ and FDR < 0.05.

Relative to the impact of PTP4A3 in standard treatment responses, *ex vivo* drug screening data from the BeatAML cohort were analyzed.[54,55] Spearman's rank correlation coefficients (r) were calculated between PTP4A3 mRNA levels and drug sensitivity scores for each compound. Statistical significance was assessed using corresponding p-values.

Cell Lines and Compounds

THP-1, U-937, HL-60, NB4, MEG-01, KG-1, OCI-AML3, HEL, MOLM-13, MV4−11, SET-2, Kasumi 1, KU-812, and K-562 cell lines were maintained according to the DSMZ (German Collection of Microorganisms and Cell Cultures, Braunschweig, Lower Saxony, Germany) and the ATCC (American Type Culture Collection, Manassas, VA, USA) guidelines and recommendations. The culture

https://doi.org/10.1021/acsptsci.6c00373
ACS Pharmacol. Transl. Sci. 2026, 9, 3217−3228

media used were RPMI 10% FBS (for THP-1, U-937, NB4, MEG-01, KG-1, HEL, MOLM-13, MV4-11, and K-562), IMDM 20% FBS (for HL-60), a-MEM 10% FBS (for OCI-AML3), and RPMI 20% (for Kasumi 1, SET-2, and KU812), all prepared with 1% penicillin/streptomycin. The cell lines, as well as their respective genetic mutations, are specified in Table S6. Cultures were routinely tested and confirmed to be mycoplasma-free during the experiments. The PTP4A3 inhibitors, JMS-053 and EJR-925, were kindly provided by Professor Peter Wipf (Department of Chemistry, University of Pittsburgh, Pittsburgh, PA, USA) and were diluted and stored in DMSO (50 mM), according to the group's instructions. PBMCs from a healthy donor were used to calculate the SI in relation to myeloid neoplasm cells. Informed consent was obtained from the healthy donor, and the Ethics Committee of the Institute of Biomedical Sciences of the University of São Paulo approved this study (Protocol number, 4423074; CAAE, 39510920.1.0000.5467). Primary PBMC were cultured in RPMI-1640 medium containing 30% FBS, penicillin/streptomycin, and recombinant cytokines (PeproTech, Cranbury, NJ, USA) (30 ng/mL IL3, 100 ng/mL IL7, 100 ng/mL FLT3-ligand, and 30 ng/mL SCF).

MTT Assay

A total of 1×10^4 cells were seeded per well in 96-well plates and cultured in the appropriate medium. Cells were then exposed to increasing concentrations (0.0032−50 μM) of the PTP4A3 inhibitors for 24, 48, or 72 h. Following treatment, 10 μL of MTT solution (5 mg/mL; Sigma-Aldrich, St. Louis, MO, USA) was added to each well, and plates were incubated at 37 °C for 4 h. The reaction was stopped by adding 150 μL of 0.1 M HCl in anhydrous isopropanol, and absorbance was measured at 570 nm using a SpectraMax M5 plate reader (Molecular Devices, San Jose, CA, USA). The resulting IC_{50} values, computed through nonlinear regression analysis in GraphPad Prism 8 software (GraphPad Software, Inc., San Diego, CA, USA), were established as reference concentrations for subsequent experiments. The SI was calculated to assess the preferential cytotoxicity of JMS-053 and EJR-925 toward leukemia cell lines compared with normal PBMCs. The SI was defined as the ratio of the IC_{50} for PBMC value to that for each leukemia cell line. SI values greater than 1.0 were considered indicative of preferential sensitivity of leukemia cells.

The sensitivity assessed by the MTT assay was integrated with PTP4A3 dependency scores obtained from AMLdb (https://project.iith.ac.in/cgntlab/amldb), enabling the evaluation of the association between treatment response and PTP4A3 dependency for cell survival. Dependency data were available for nine AML cell lines included in our viability assays and were therefore used for the correlation analyses, as detailed in Table S5. The dependency scores (DS) available in AMLdb were originally derived from the DepMap project (Broad Institute, Cambridge, MA, USA).

For drug combination studies, THP-1 and U-937 cells were treated with graded doses below the IC_{50} values of the compounds JMS-053 (0−8 μM for THP-1; 0−4 μM for U-937), venetoclax (0−5 μM for THP-1; 0−3 μM for U-937), and cytarabine (0−500 nM for THP-1; 0−52 nM for U-937), either alone or in combination, for 72 h. Data visualization was performed using the Multiple Experiment Viewer (MeV) 4.9.0 software (TM4, Boston, MA, USA), and the ZIP synergy score was calculated using SynergyFinder (https://synergyfinder.fimm.fi/).

Quantitative PCR (qPCR)

Samples containing 1 μg of RNA from AML cell lines were reverse transcribed into cDNA using the High-Capacity cDNA Archive Kit (Thermo Fisher Scientific, San Jose, CA, USA). Gene amplification was performed on a QuantStudio 3 Real-Time PCR System using Power SYBR Green PCR Master Mix (Thermo Fisher Scientific). A total of 60 nanograms of cDNA from each of the three biological replicates were used for the analysis. A negative control, in which cDNA was replaced with RNase-free water, was included for each primer pair. The reference genes were HPRT1 and ACTB, and relative expression was calculated using the $2^{-\Delta\Delta CT}$ method.[56] The primers are listed in Table S7. A no-template control was included for each primer pair to verify the absence of contamination. To assess the specificity, a dissociation curve analysis was conducted at the end of each run. PTP4A3 expression levels were combined with MTT assay results to determine the correlation between gene expression and sensitivity to its inhibitors.

Clonogenic Assay

For the colony formation assay, THP-1, U-937, and HL-60 cells were seeded in semisolid methylcellulose medium (MethoCult H4230, STEMCELL Technologies, Vancouver, British Columbia, Canada) at a density of 1×10^3 cells/mL in 12-well plates and exposed to either vehicle or JMS-053 and EJR-925 at concentrations of 1.25−20 μM. The plates were incubated at 37 °C, 5% CO_2, and assessments were carried out after 7−10 days of treatment. Colonies were detected with the addition of 100 μL (5 mg/mL) of MTT, recorded by images generated using the G:BOX Chemi XRQ equipment (Syngene, Cambridge, U.K.) and counted using ImageJ software (U.S. National Institutes of Health, Bethesda, MD, USA).

Apoptosis Assessment

THP-1, U-937, and HL-60 cells were seeded at a density of 1×10^5 cells/well in 24-well plates and treated with vehicle or JMS-053 and EJR-925 in the ranges of 1.25−10 μM. Cells were incubated for 48 h, then washed twice with cold PBS and resuspended in a binding buffer containing 0.5 μg/mL propidium iodide (PI; Sigma-Aldrich) and 2.5 μg/mL annexin V-APC (BD Pharmingen, San Diego, CA, USA). Samples were incubated for 15 min at room temperature protected from light, followed by flow cytometry analysis using a FACSCalibur system (Becton Dickinson, Lincoln Park, NJ, USA). Data were analyzed with FlowJo software (Tree Star Inc., Ashland, OR, USA).

Cell Cycle Analysis

The THP-1, U-937, and HL-60 cell lines were seeded at a density of 2×10^5 cells/well in 12-well plates and treated with 1.25−10 μM JMS-053 or EJR-925 for 48 h. Cells were washed with PBS and resuspended in 100 μL of PBS, followed by the addition of 75% ethanol (900 μL) and temporary storage at 4 °C (at least 24 h). After centrifugation at 1200 rpm for 5 min, the supernatant was discarded, and the cells were washed again with PBS. The pellet was resuspended in 300 μL of staining solution containing 0.1% Triton X-100, 100 μg/mL RNase (50 mg/mL; Merck, Darmstadt, Hessen, Germany), and 10 μg/mL propidium iodide (500 μg/mL; Sigma-Aldrich). Cells were incubated for 30 min, protected from light, and analyzed on a BD FACSCalibur flow cytometer, acquiring 10,000 events per condition.

Protein Extraction and Western Blot

THP-1 and U-937 cells were treated with the compounds JMS-053 or EJR-925 (1.25−10 μM) for 24 h. A new set of treatments was performed at 0, 3, 6, 9, 12, and 24 h at a concentration of 10 μM to evaluate the time−response relationship of both compounds. Total proteins were extracted using a buffer containing 100 mM Tris (pH 7.6), 1% Triton X-100, 2 mM PMSF, 10 mM Na_3VO_4, 100 mM NaF, 10 mM $Na_4P_2O_7$, and 10 mM EDTA. Equal amounts of total protein (30 μg) were subjected to SDS-PAGE and Western blot with antibodies listed in Table S8. Signal detection used SuperSignal West Dura Extended Duration Substrate (Thermo Fisher Scientific) and Gel Doc XR+ system (Bio-Rad, Hercules, CA, USA). Images were captured using the G:BOX Chemi system (Syngene, Cambridge, U.K.) and quantified with UN-SCAN-IT gel 6.1 software (Silk Scientific, Orem, UT, USA). Protein content was normalized to α-tubulin expression.

Statistical Analyses

Statistical analyses were performed using GraphPad Prism 8. Comparisons between groups were conducted using Student's t test, one-way ANOVA followed by Bonferroni's post hoc test, or the Kruskal−Wallis test followed by Dunn's post hoc test, as appropriate. Spearman correlation coefficients were calculated to assess the strength and direction of associations between PTP4A3 expression and genes of interest. Overall survival (OS) was calculated as the difference in months between diagnosis and the last follow-up or death, and disease-free survival (DFS) between the date of complete remission and relapse or the date of the last follow-up or death (which

https://doi.org/10.1021/acsptsci.6c00373
ACS Pharmacol. Transl. Sci. 2026, 9, 3217−3228

occurred first). Survival analyses were performed using the Kaplan–Meier method, Log-rank test, and Cox proportional hazards regression, comparing groups with low versus high PTP4A3 expression. A value of $p < 0.05$ was considered statistically significant.

CONCLUSION

In conclusion, this study identifies PTP4A3 as a clinically relevant biomarker and potential therapeutic target in AML. High PTP4A3 expression was associated with adverse prognosis, poorly differentiated leukemic populations, activation of oncogenic and inflammatory signaling pathways, and resistance to antileukemic therapies. Importantly, pharmacological inhibition of PTP4A3 reduced AML cell viability and clonogenicity, induced apoptosis and DNA damage, suppressed ERK1/2 activation, and potentiated the effects of cytarabine and venetoclax. Collectively, our findings support a clinically and biologically relevant, context-dependent role for PTP4A3 in AML, highlighting its potential as a prognostic biomarker and pharmacological target in selected disease contexts.

ASSOCIATED CONTENT

Data Availability Statement

The data sets generated and/or analyzed during the current study are available from the corresponding authors on reasonable request.

Supporting Information

The Supporting Information is available free of charge at https://pubs.acs.org/doi/10.1021/acsptsci.6c00373.

Additional experimental details, materials, and methods, including technical information about the cell lines, antibodies, and primers used, and results for the viability and clonogenic assays, univariate and multivariate analysis, and CIBERSORTx (PDF)

AUTHOR INFORMATION

Corresponding Authors

Natália Sudan Parducci − *Department of Pharmacology, Institute of Biomedical Sciences, University of São Paulo, São Paulo CEP 05508-900, Brazil*; Email: nataliasudanparducci@gmail.com

João Agostinho Machado-Neto − *Department of Pharmacology, Institute of Biomedical Sciences, University of São Paulo, São Paulo CEP 05508-900, Brazil*; orcid.org/0000-0002-2937-8109; Email: jamachadoneto@usp.br

Authors

Maria Fernanda Lopes Carvalho − *Department of Pharmacology, Institute of Biomedical Sciences, University of São Paulo, São Paulo CEP 05508-900, Brazil*

Isabelle Caroline Santos − *Department of Pharmacology, Institute of Biomedical Sciences, University of São Paulo, São Paulo CEP 05508-900, Brazil*; orcid.org/0009-0005-2373-0502

Letícia Machado Favery Bertoline − *Department of Pharmacology, Institute of Biomedical Sciences, University of São Paulo, São Paulo CEP 05508-900, Brazil*

Giovanna A. Castro − *Department of Computer Science, Federal University of São Carlos (UFSCar), Sorocaba, São Paulo 18052-780, Brazil*

Juan Luiz Coelho-Silva − *Department of Pharmacology, Institute of Biomedical Sciences, University of São Paulo, São Paulo CEP 05508-900, Brazil*

Tiago Agostinho Almeida − *Department of Computer Science, Federal University of São Carlos (UFSCar), Sorocaba, São Paulo 18052-780, Brazil*

Peter Wipf − *Department of Chemistry, University of Pittsburgh, Pittsburgh, Pennsylvania 15260, United States*; orcid.org/0000-0001-7693-5863

Complete contact information is available at: https://pubs.acs.org/10.1021/acsptsci.6c00373

Author Contributions

N.S.P. conceived and conducted the study, performing the *in vitro* experiments, data collection, analysis, and interpretation. She also prepared the reports and drafted the manuscript. M.F.L.C. contributed to study conceptualization, selection of the primary gene of interest, bioinformatics analyses, *in vitro* experiments, and manuscript preparation. L.M.F.B. contributed to the bioinformatics analysis, execution of *in vitro* experiments, and manuscript preparation. I.C.S. and J.L.C.-S. contributed to additional *in silico* analyses, supporting the project through their programming expertise, and reviewed the manuscript. G.A.C. and T.A.A. performed the initial AI-based mapping of genes associated with disease prognosis, contributing to the definition of the study focus and manuscript review. P.W. provided the inhibitors used in this study, which were previously developed and characterized by his research group, and also reviewed the manuscript. J.A.M.-N. supervised the research and served as the principal investigator of the laboratory. All authors reviewed and approved the final version of the manuscript.

Funding

The Article Processing Charge for the publication of this research was funded by the Coordenacao de Aperfeicoamento de Pessoal de Nivel Superior (CAPES), Brazil (ROR identifier: 00x0ma614).

Notes

The authors declare no competing financial interest.

ACKNOWLEDGMENTS

N.S.P., M.F.L.C., L.M.F.B., I.C.S., and J.L.C.S. received fellowships from São Paulo Research Foundation (FAPESP; Grants 2025/07801-6, 2023/12969-8, 2024/07906-0, 2025/23622-4, and 2024/21624-7). This study was supported by Grants 2021/11606-3, 2023/12246-6, and 2023/08735-1 also from the FAPESP, by Grant 305758/2021-7 from Conselho Nacional de Desenvolvimento Científico e Tecnológico (CNPq), and by the Coordenação de Aperfeiçoamento de Pessoal de Nível Superior, Brasil (CAPES), Finance Code 001.

ABBREVIATIONS

AI, artificial intelligence; AKT, protein kinase B; AML, acute myeloid leukemia; ANOVA, analysis of variance; APL, acute promyelocytic leukemia; ATCC, American Type Culture Collection; AUC, area under the curve; B-ALL, B-cell acute lymphoblastic leukemia; C-index, concordance index; CMP, common myeloid progenitor; CRISPR, clustered regularly interspaced short palindromic repeats; DEGs, differentially expressed genes; DFS, disease-free survival; DS, dependency score; DSMZ, German Collection of Microorganisms and Cell

https://doi.org/10.1021/acsptsci.6c00373
ACS Pharmacol. Transl. Sci. 2026, 9, 3217−3228

Cultures; ERK1/2, extracellular signal-regulated kinases 1 and 2; ES, enrichment score; FC, fold change; FDR, false discovery rate; FLT3, FMS-like tyrosine kinase 3; FLT3-ITD, FMS-like tyrosine kinase 3 internal tandem duplication; GMP, granulocyte−monocyte progenitor; GO, gene ontology; GSEA, Gene Set Enrichment Analysis; HR, hazard ratio; HSC, hematopoietic stem cell; IC50, half-maximal inhibitory concentration; LSPC, leukemic stem and progenitor cell; MAPK, mitogen-activated protein kinase; MEP, megakaryocyte-erythroid progenitor; ML, machine learning; MPP, multipotential progenitor; MTT, methylthiazolyl tetrazolium; NES, normalized enrichment score; NF-κB, nuclear factor kappa B; NK, normal karyotype; OS, overall survival; PBMC, peripheral blood mononuclear cell; PI, propidium iodide; PI3K, phosphatidylinositol 3-kinase; PRL-3, phosphatase of regenerating liver 3; PTP4A3, protein tyrosine phosphatase 4A3; qPCR, quantitative polymerase chain reaction; ROC, receiver operating characteristic; SI, selectivity index; TCGA, The Cancer Genome Atlas; TNF-α, tumor necrosis factor alpha; TNFR1, tumor necrosis factor receptor 1; WGCNA, Weighted Gene Coexpression Network Analysis; ZIP, zero interaction potency.

REFERENCES

(1) Hanahan, D. Hallmarks of Cancer: New Dimensions. *Cancer Discov.* **2022**, *12*, 31−46.

(2) Hanahan, D.; Weinberg, R. A. Hallmarks of cancer: the next generation. *Cell* **2011**, *144*, 646−674.

(3) Alshuhri, S. M.; Al-Musawi, S. G.; Al-Alwany, A. A.; Uinarni, H.; Rasulova, I.; Rodrigues, P.; Alkhafaji, A. T.; Alshanberi, A. M.; Alawadi, A. H.; Abbas, A. H. Artificial intelligence in cancer diagnosis: Opportunities and challenges. *Pathol. Res. Pract.* **2024**, *253*, No. 154996.

(4) Zhang, B.; Shi, H.; Wang, H. Machine Learning and AI in Cancer Prognosis, Prediction, and Treatment Selection: A Critical Approach. *J. Multidiscip. Healthc.* **2023**, *16*, 1779−1791.

(5) Sherani, A. M. K.; Khan, M.; Qayyum, M. U.; Hussain, H. K. Synergizing AI and Healthcare: Pioneering Advances in Cancer Medicine for Personalized Treatment. *International Journal of Multidisciplinary Sciences and Arts* **2024**, *3*, 270−277.

(6) Gupta, S.; Gupta, M. K.; Shabaz, M.; Sharma, A. Deep learning techniques for cancer classification using microarray gene expression data. *Front. Physiol.* **2022**, *13*, No. 952709.

(7) Alhajahjeh, A.; Nazha, A. Unlocking the Potential of Artificial Intelligence in Acute Myeloid Leukemia and Myelodysplastic Syndromes. *Curr. Hematol. Malig. Rep.* **2024**, *19*, 9−17.

(8) Gimeno, M.; San Jose-Eneriz, E.; Villar, S.; Agirre, X.; Prosper, F.; Rubio, A.; Carazo, F. Explainable artificial intelligence for precision medicine in acute myeloid leukemia. *Front. Immunol.* **2022**, *13*, No. 977358.

(9) Deschler, B.; Lubbert, M. Acute myeloid leukemia: epidemiology and etiology. *Cancer* **2006**, *107*, 2099−2107.

(10) Coelho-Silva, J. L.; Parducci, N. S.; Carvalho, M. F. L.; Vahedian, V.; Lima, K.; de Almeida, B. O.; Machado-Neto, J. A. Targeting "undruggable" cancer proteins: pharmacological challenges and emerging strategies. *Transl. Cancer Res.* **2026**, *15*, 336.

(11) Castro, G. A.; Almeida, J. M.; Machado-Neto, J. A.; Almeida, T. A. A decision support system to recommend appropriate therapy protocol for AML patients. *Front. Artif. Intell.* **2024**, *7*, No. 1343447.

(12) Sharlow, E. R.; Wipf, P.; McQueeney, K. E.; Bakan, A.; Lazo, J. S. Investigational inhibitors of PTP4A3 phosphatase as antineoplastic agents. *Expert. Opin. Investig. Drugs* **2014**, *23*, 661−673.

(13) Bessette, D. C.; Qiu, D.; Pallen, C. J. PRL PTPs: mediators and markers of cancer progression. *Cancer Metastasis Rev.* **2008**, *27*, 231−252.

(14) Yeh, H. C.; Li, C. C.; Huang, C. N.; Hour, T. C.; Yeh, B. W.; Li, W. M.; Liang, P. I.; Chang, L. L.; Li, C. F.; Wu, W. J. PTP4A3 Independently Predicts Metastasis and Survival in Upper Tract Urothelial Carcinoma Treated with Radical Nephroureterectomy. *J. Urol.* **2015**, *194*, 1449−1455.

(15) McQueeney, K. E.; Salamoun, J. M.; Ahn, J. G.; Pekic, P.; Blanco, I. K.; Struckman, H. L.; Sharlow, E. R.; Wipf, P.; Lazo, J. S. A chemical genetics approach identifies PTP4A3 as a regulator of colon cancer cell adhesion. *FASEB J.* **2018**, *32*, 5661−5673.

(16) Lazo, J. S.; Sharlow, E. R.; Cornelison, R.; Hart, D. J.; Llaneza, D. C.; Mendelson, A. J.; Rastelli, E. J.; Tasker, N. R.; Landen, C. N.; Wipf, P. Credentialing and Pharmacologically Targeting PTP4A3 Phosphatase as a Molecular Target for Ovarian Cancer. *Biomolecules* **2021**, *11*, 969.

(17) Lian, Y. X.; Chen, R.; Xu, Y. H.; Peng, C. L.; Hu, H. C. Effect of protein-tyrosine phosphatase 4A3 by small interfering RNA on the proliferation of lung cancer. *Gene* **2012**, *511*, 169−176.

(18) den Hollander, P.; Rawls, K.; Tsimelzon, A.; Shepherd, J.; Mazumdar, A.; Hill, J.; Fuqua, S. A.; Chang, J. C.; Osborne, C. K.; Hilsenbeck, S. G.; Mills, G. B.; Brown, P. H. Phosphatase PTP4A3 Promotes Triple-Negative Breast Cancer Growth and Predicts Poor Patient Survival. *Cancer Res.* **2016**, *76*, 1942−1953.

(19) Jin, X.; Shi, H.; Li, Z.; Li, H.; Ma, H.; Shi, X. Characterizing PTP4A3/PRL-3 as the Potential Prognostic Marker Gene for Liver Hepatocellular Carcinoma. *J. Oncol.* **2022**, *2022*, No. 2717056.

(20) Laurent, C.; Valet, F.; Planque, N.; Silveri, L.; Maacha, S.; Anezo, O.; Hupe, P.; Plancher, C.; Reyes, C.; Albaud, B.; Rapinat, A.; Gentien, D.; Couturier, J.; Sastre-Garau, X.; Desjardins, L.; Thiery, J. P.; Roman-Roman, S.; Asselain, B.; Barillot, E.; Piperno-Neumann, S.; Saule, S. High PTP4A3 phosphatase expression correlates with metastatic risk in uveal melanoma patients. *Cancer Res.* **2011**, *71*, 666−674.

(21) Song, Q.; Zheng, Y.; Wu, J.; Wang, S.; Meng, L.; Yao, Q.; Li, Z.; Lian, S. PTP4A3 Is a Prognostic Biomarker Correlated With Immune Infiltrates in Papillary Renal Cell Carcinoma. *Front. Immunol.* **2021**, *12*, No. 717688.

(22) Wei, M.; Haney, M. G.; Rivas, D. R.; Blackburn, J. S. Protein tyrosine phosphatase 4A3 (PTP4A3/PRL-3) drives migration and progression of T-cell acute lymphoblastic leukemia in vitro and in vivo. *Oncogenesis* **2020**, *9*, 6.

(23) Guo, K.; Li, J.; Tang, J. P.; Koh, V.; Gan, B. Q.; Zeng, Q. Catalytic domain of PRL-3 plays an essential role in tumor metastasis: formation of PRL-3 tumors inside the blood vessels. *Cancer Biol. Ther* **2004**, *3*, 945−951.

(24) Bardelli, A.; Saha, S.; Sager, J. A.; Romans, K. E.; Xin, B.; Markowitz, S. D.; Lengauer, C.; Velculescu, V. E.; Kinzler, K. W.; Vogelstein, B. PRL-3 expression in metastatic cancers. *Clin. Cancer Res.* **2003**, *9*, 5607−5615.

(25) Zhou, J.; Bi, C.; Chng, W. J.; Cheong, L. L.; Liu, S. C.; Mahara, S.; Tay, K. G.; Zeng, Q.; Li, J.; Guo, K.; Tan, C. P.; Yu, H.; Albert, D. H.; Chen, C. S. PRL-3, a metastasis associated tyrosine phosphatase, is involved in FLT3-ITD signaling and implicated in anti-AML therapy. *PLoS One* **2011**, *6*, No. e19798.

(26) Rastelli, E. J.; Sannino, S.; Hart, D. J.; Sharlow, E. R.; Lazo, J. S.; Brodsky, J. L.; Wipf, P. Synthesis and evaluation of bifunctional PTP4A3 phosphatase inhibitors activating the ER stress pathway. *Bioorg. Med. Chem. Lett.* **2021**, *46*, No. 128167.

(27) Wei, M.; Korotkov, K. V.; Blackburn, J. S. Targeting phosphatases of regenerating liver (PRLs) in cancer. *Pharmacol. Ther.* **2018**, *190*, 128−138.

(28) McQueeney, K. E.; Salamoun, J. M.; Burnett, J. C.; Barabutis, N.; Pekic, P.; Lewandowski, S. L.; Llaneza, D. C.; Cornelison, R.; Bai, Y.; Zhang, Z. Y.; Catravas, J. D.; Landen, C. N.; Wipf, P.; Lazo, J. S.; Sharlow, E. R. Targeting ovarian cancer and endothelium with an allosteric PTP4A3 phosphatase inhibitor. *Oncotarget* **2018**, *9*, 8223−8240.

(29) Lazo, J. S.; Blanco, I. K.; Tasker, N. R.; Rastelli, E. J.; Burnett, J. C.; Garrott, S. R.; Hart, D. J.; McCloud, R. L.; Hsu, K. L.; Wipf, P.; Sharlow, E. R. Next-Generation Cell-Active Inhibitors of the Undrugged Oncogenic PTP4A3 Phosphatase. *J. Pharmacol. Exp. Ther.* **2019**, *371*, 652−662.

https://doi.org/10.1021/acsptsci.6c00373
ACS Pharmacol. Transl. Sci. 2026, 9, 3217−3228

(30) Daneshbod, Y.; Kohan, L.; Taghadosi, V.; Weinberg, O. K.; Arber, D. A. Prognostic Significance of Complex Karyotypes in Acute Myeloid Leukemia. *Curr. Treat. Options Oncol.* **2019**, *20*, 15.
(31) Daver, N.; Schlenk, R. F.; Russell, N. H.; Levis, M. J. Targeting FLT3 mutations in AML: review of current knowledge and evidence. *Leukemia* **2019**, *33*, 299−312.
(32) Park, J. E.; Yuen, H. F.; Zhou, J. B.; Al-Aidaroos, A. Q.; Guo, K.; Valk, P. J.; Zhang, S. D.; Chng, W. J.; Hong, C. W.; Mills, K.; Zeng, Q. Oncogenic roles of PRL-3 in FLT3-ITD induced acute myeloid leukaemia. *EMBO Mol. Med.* **2013**, *5*, 1351−1366.
(33) Kottaridis, P. D.; Gale, R. E.; Linch, D. C. Prognostic implications of the presence of FLT3 mutations in patients with acute myeloid leukemia. *Leuk Lymphoma* **2003**, *44*, 905−913.
(34) Ketley, N. J.; Allen, P. D.; Kelsey, S. M.; Newland, A. C. Mechanisms of resistance to apoptosis in human AML blasts: the role of differentiation-induced perturbations of cell-cycle checkpoints. *Leukemia* **2000**, *14*, 620−628.
(35) Schuringa, J. J.; Wierenga, A. T.; Kruijer, W.; Vellenga, E. Constitutive Stat3, Tyr705, and Ser727 phosphorylation in acute myeloid leukemia cells caused by the autocrine secretion of interleukin-6. *Blood* **2000**, *95*, 3765−3770.
(36) Wang, M.; Zhang, C.; Tian, T.; Zhang, T.; Wang, R.; Han, F.; Zhong, C.; Hua, M.; Ma, D. Increased Regulatory T Cells in Peripheral Blood of Acute Myeloid Leukemia Patients Rely on Tumor Necrosis Factor (TNF)-alpha-TNF Receptor-2 Pathway. *Front. Immunol.* **2018**, *9*, 1274.
(37) Wingelhofer, B.; Maurer, B.; Heyes, E. C.; Cumaraswamy, A. A.; Berger-Becvar, A.; de Araujo, E. D.; Orlova, A.; Freund, P.; Ruge, F.; Park, J.; Tin, G.; Ahmar, S.; Lardeau, C. H.; Sadovnik, I.; Bajusz, D.; Keseru, G. M.; Grebien, F.; Kubicek, S.; Valent, P.; Gunning, P. T.; Moriggl, R. Pharmacologic inhibition of STAT5 in acute myeloid leukemia. *Leukemia* **2018**, *32*, 1135−1146.
(38) Mustafa Ali, M. K.; Williams, M. T.; Corley, E. M.; AlKaabba, F.; Niyongere, S. Impact of KRAS and NRAS mutations on outcomes in acute myeloid leukemia. *Leuk. Lymphoma* **2023**, *64*, 962−971.
(39) Hjort, M. A.; Abdollahi, P.; Vandsemb, E. N.; Fenstad, M. H.; Lund, B.; Slordahl, T. S.; Borset, M.; Ro, T. B. Phosphatase of regenerating liver-3 is expressed in acute lymphoblastic leukemia and mediates leukemic cell adhesion, migration and drug resistance. *Oncotarget* **2018**, *9*, 3549−3561.
(40) Zhou, J.; Toh, S. H.; Chan, Z. L.; Quah, J. Y.; Chooi, J. Y.; Tan, T. Z.; Chong, P. S. Y.; Zeng, Q.; Chng, W. J. A loss-of-function genetic screening reveals synergistic targeting of AKT/mTOR and WTN/beta-catenin pathways for treatment of AML with high PRL-3 phosphatase. *J. Hematol. Oncol.* **2018**, *11*, 36.
(41) Du, Y.; Zhang, X. F.; Wu, S.; Zheng, J.; Gao, H.; Xi, S.; Sun, L.; Yan, J.; Wang, F.; Wang, Y.; Yang, H.; Ou, X.; Liu, M.; Xiao, J.; Pan, Q.; Li, Y. PTP4A3 dephosphorylates EGFR to promote metastasis and enhance sensitivity to lapatinib in hepatocellular carcinoma. *Oncogene* **2026**, *45*, 3385−3400.
(42) Gari, H. H.; DeGala, G. D.; Lucia, M. S.; Lambert, J. R. Loss of the oncogenic phosphatase PRL-3 promotes a TNF-R1 feedback loop that mediates triple-negative breast cancer growth. *Oncogenesis* **2016**, *5*, e255.
(43) Wang, L.; Liu, J.; Zhong, Z.; Gong, X.; Liu, W.; Shi, L.; Li, X. PTP4A3 is a target for inhibition of cell proliferatin, migration and invasion through Akt/mTOR signaling pathway in glioblastoma under the regulation of miR-137. *Brain Res.* **2016**, *1646*, 441−450.
(44) Salamoun, J. M.; McQueeney, K. E.; Patil, K.; Geib, S. J.; Sharlow, E. R.; Lazo, J. S.; Wipf, P. Photooxygenation of an amino-thienopyridone yields a more potent PTP4A3 inhibitor. *Org. Biomol. Chem.* **2016**, *14*, 6398−6402.
(45) Harris, P.; Ralph, P. Human leukemic models of myelomonocytic development: a review of the HL-60 and U937 cell lines. *J. Leukoc. Biol.* **1985**, *37*, 407−422.
(46) Drexler, H. G.; Quentmeier, H.; MacLeod, R. A.; Uphoff, C. C.; Hu, Z. B. Leukemia cell lines: in vitro models for the study of acute promyelocytic leukemia. *Leuk Res.* **1995**, *19*, 681−691.
(47) Jiang, Y.; Liu, X. Q.; Rajput, A.; Geng, L.; Ongchin, M.; Zeng, Q.; Taylor, G. S.; Wang, J. Phosphatase PRL-3 is a direct regulatory target of TGFbeta in colon cancer metastasis. *Cancer Res.* **2011**, *71*, 234−244.
(48) Chong, P. S. Y.; Zhou, J.; Chooi, J. Y.; Chan, Z. L.; Toh, S. H. M.; Tan, T. Z.; Wee, S.; Gunaratne, J.; Zeng, Q.; Chng, W. J. Non-canonical activation of beta-catenin by PRL-3 phosphatase in acute myeloid leukemia. *Oncogene* **2019**, *38*, 1508−1519.
(49) Zhang, H.; Kozlov, G.; Li, X.; Wu, H.; Gulerez, I.; Gehring, K. PRL3 phosphatase active site is required for binding the putative magnesium transporter CNNM3. *Sci. Rep.* **2017**, *7*, 48.
(50) Oh, M. H.; Jang, J.; Lee, J. H. Polarization of THP-1-Derived Macrophage by Magnesium and MAGT1 Inhibition in Wound Healing. *Arch. Plast. Surg.* **2023**, *50*, 432−442.
(51) Thiele, C.; Hirschfeld, G. cutpointr: Improved Estimation and Validation of Optimal Cutpoints in *R. J. Stat. Soft.* **2021**, *98*. DOI: 10.18637/jss.v098.i11.
(52) Langfelder, P.; Horvath, S. WGCNA: an R package for weighted correlation network analysis. *BMC Bioinformatics* **2008**, *9*, 559.
(53) Yu, G.; Wang, L. G.; Han, Y.; He, Q. Y. clusterProfiler: an R package for comparing biological themes among gene clusters. *OMICS* **2012**, *16*, 284−287.
(54) Tyner, J. W.; Tognon, C. E.; Bottomly, D.; Wilmot, B.; Kurtz, S. E.; Savage, S. L.; Long, N.; Schultz, A. R.; Traer, E.; Abel, M.; Agarwal, A.; Blucher, A.; Borate, U.; Bryant, J.; Burke, R.; Carlos, A.; Carpenter, R.; Carroll, J.; Chang, B. H.; Coblentz, C.; d'Almeida, A.; Cook, R.; Danilov, A.; Dao, K. T.; Degnin, M.; Devine, D.; Dibb, J.; Edwards, D. K. t.; Eide, C. A.; English, I.; Glover, J.; Henson, R.; Ho, H.; Jemal, A.; Johnson, K.; Johnson, R.; Junio, B.; Kaempf, A.; Leonard, J.; Lin, C.; Liu, S. Q.; Lo, P.; Loriaux, M. M.; Luty, S.; Macey, T.; MacManiman, J.; Martinez, J.; Mori, M.; Nelson, D.; Nichols, C.; Peters, J.; Ramsdill, J.; Rofelty, A.; Schuff, R.; Searles, R.; Segerdell, E.; Smith, R. L.; Spurgeon, S. E.; Sweeney, T.; Thapa, A.; Visser, C.; Wagner, J.; Watanabe-Smith, K.; Werth, K.; Wolf, J.; White, L.; Yates, A.; Zhang, H.; Cogle, C. R.; Collins, R. H.; Connolly, D. C.; Deininger, M. W.; Drusbosky, L.; Hourigan, C. S.; Jordan, C. T.; Kropf, P.; Lin, T. L.; Martinez, M. E.; Medeiros, B. C.; Pallapati, R. R.; Pollyea, D. A.; Swords, R. T.; Watts, J. M.; Weir, S. J.; Wiest, D. L.; Winters, R. M.; McWeeney, S. K.; Druker, B. J. Functional genomic landscape of acute myeloid leukaemia. *Nature* **2018**, *562*, 526−531.
(55) Bottomly, D.; Long, N.; Schultz, A. R.; Kurtz, S. E.; Tognon, C. E.; Johnson, K.; Abel, M.; Agarwal, A.; Avaylon, S.; Benton, E.; Blucher, A.; Borate, U.; Braun, T. P.; Brown, J.; Bryant, J.; Burke, R.; Carlos, A.; Chang, B. H.; Cho, H. J.; Christy, S.; Coblentz, C.; Cohen, A. M.; d'Almeida, A.; Cook, R.; Danilov, A.; Dao, K. T.; Degnin, M.; Dibb, J.; Eide, C. A.; English, I.; Hagler, S.; Harrelson, H.; Henson, R.; Ho, H.; Joshi, S. K.; Junio, B.; Kaempf, A.; Kosaka, Y.; Laderas, T.; Lawhead, M.; Lee, H.; Leonard, J. T.; Lin, C.; Lind, E. F.; Liu, S. Q.; Lo, P.; Loriaux, M. M.; Luty, S.; Maxson, J. E.; Macey, T.; Martinez, J.; Minnier, J.; Monteblanco, A.; Mori, M.; Morrow, Q.; Nelson, D.; Ramsdill, J.; Rofelty, A.; Rogers, A.; Romine, K. A.; Ryabinin, P.; Saultz, J. N.; Sampson, D. A.; Savage, S. L.; Schuff, R.; Searles, R.; Smith, R. L.; Spurgeon, S. E.; Sweeney, T.; Swords, R. T.; Thapa, A.; Thiel-Klare, K.; Traer, E.; Wagner, J.; Wilmot, B.; Wolf, J.; Wu, G.; Yates, A.; Zhang, H.; Cogle, C. R.; Collins, R. H.; Deininger, M. W.; Hourigan, C. S.; Jordan, C. T.; Lin, T. L.; Martinez, M. E.; Pallapati, R. R.; Pollyea, D. A.; Pomicter, A. D.; Watts, J. M.; Weir, S. J.; Druker, B. J.; McWeeney, S. K.; Tyner, J. W. Integrative analysis of drug response and clinical outcome in acute myeloid leukemia. *Cancer Cell* **2022**, *40*, 850−864.
(56) Livak, K. J.; Schmittgen, T. D. Analysis of relative gene expression data using real-time quantitative PCR and the 2(-Delta Delta C(T)) Method. *Methods* **2001**, *25*, 402−408.